Understanding Rate-Limiting Processes for the Sublimation of Small Molecule Organic Semiconductors

Nathan T. Morgan and Yi Zhang
Dept. of Chemical Engineering and Materials Science, University of Minnesota, Minneapolis, MN 55455

Erich J. Molitor
Engineering and Process Sciences, Core R&D, The Dow Chemical Company, Midland, MI 48674

Bruce M. Bell
Analytical Sciences, Core R&D, The Dow Chemical Company, Midland, MI 48674

Russell J. Holmes and E. L. Cussler
Dept. of Chemical Engineering and Materials Science, University of Minnesota, Minneapolis, MN 55455

DOI 10.1002/aic.14357
Published online January 27, 2014 in Wiley Online Library (wileyonlinelibrary.com)

Organic small molecules continue to gain attention for application in light-emitting devices in displays and solid-state lighting. The purification of these materials by sublimation represents a critical obstacle for their high throughput processing. In this work, we find that the purification of the archetypical hole-transporting material N,N′-bis(naphthalen-1-yl)-N,N′-bis(phenyl)-benzidine (α-NPD) is controlled by a combination of viscous flow, Knudsen diffusion, and physical vapor deposition. In contrast with other commercially practiced sublimations, steps like diffusion within the solid feed, desorption from the feed particle surface, and mass transfer within the bed of feed particles, do not significantly affect the sublimation rate. This work provides guidelines for the large-scale purification of organic semiconductor materials, and possibly for a broader range of high value small molecule specialty materials. © 2014 American Institute of Chemical Engineers *AIChE J*, 60: 1347–1354, 2014

Keywords: sublimation, purification, organic semiconductors, organic electronics, organic light-emitting devices

Introduction

Since the first report of an organic light-emitting device (OLED) by Tang and VanSlyke,[1] there has been intense research into the development of novel materials and device architectures for the realization of high luminescence efficiencies and long device lifetimes.[2,3] Less attention has been directed to the development of techniques to realize the large-scale synthesis and processing of these materials at the level needed for widespread adoption in display and solid-state lighting technologies. Currently, most commercially available OLED displays use small molecule, low molecular weight organic semiconductors that are purified using thermal gradient sublimation,[4,5] shown schematically in Figure 1. In this method, the crude material is heated in an open container called a "boat." Vapor flows out of the boat down the collection tube until it deposits on a colder part of the tube wall, where it is manually collected. Although this method can often be used to realize high material purity, it is slow, has low-throughput, and may be subject to substantial run-to-run variations.

In this work, we report detailed sublimation experiments for the archetypical hole transport material N,N′-bis(naphthalene-1-yl)-N,N′-bis(phenyl)-benzidine (α-NPD).[6–9] Rate-controlling mechanisms are elucidated by characterizing how the sublimation rate varies with purity, system geometry, and treatment time. With a model describing the sublimation of α-NPD and the relevant rate-controlling steps, we show how these mechanisms can be modified and extended to large scale production.

Theory

The controlling rate in the sublimation process is the product of the key surface area involved and the flux. The product of the area and the flux, integrated over time, is the mass sublimed or yield of the process. Here, eight possible rate-limiting mechanisms are analyzed in significant detail, based on those observed for other systems throughout the literature.[10–17] These mechanisms are shown schematically in Figure 1, and the corresponding areas and fluxes for each of these mechanisms are summarized in Table 1. For the case where the system is limited by mass transfer from the boat to the collection zone, there are three specific mechanisms which are discussed in detail below. A discussion of the other mechanisms in Table 1 is available in Supporting Information.

The first mechanism where mass transfer in the tube from the hot vapor to the cold collection zone controls the sublimation rate is sometimes called the Hertz–Knudsen limit (6a in Table 1).[15–17] The flux j_1 is simply the product of the vapor concentration c_1 and the molecular velocity u_1

Additional Supporting Information may be found in the online version of this article.

Correspondence concerning this article should be addressed to R. J. Holmes at rholmes@umn.edu.

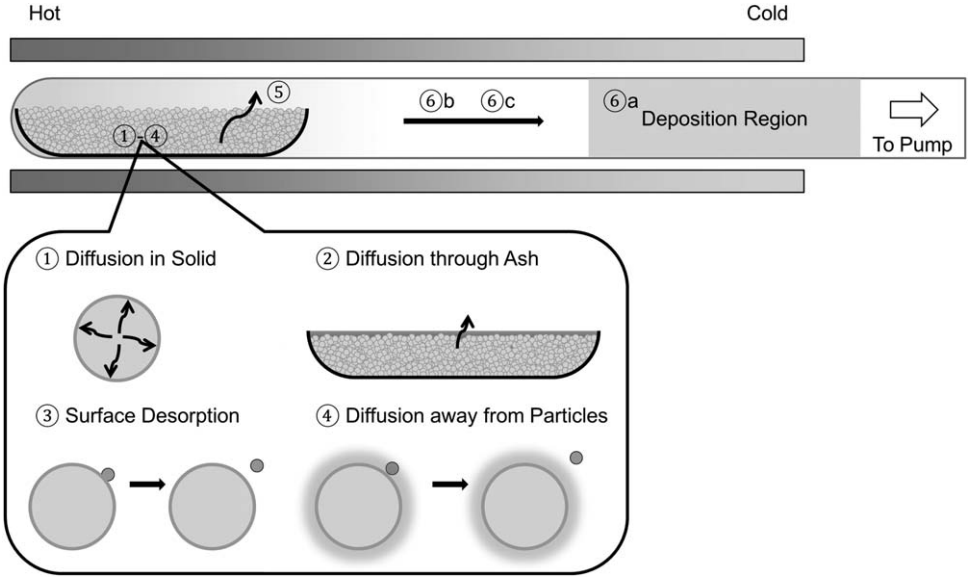

Figure 1. Sublimation system schematic and illustration of rate-limiting steps in a vacuum sublimation process.

The numbers correspond to the mechanisms listed in Table 1.

$$j_1 = \frac{(c_1)[u_1]}{4} = \frac{1}{4}\left(\frac{p_1 m_1}{k_B T}\right)\left[\sqrt{\frac{8k_B T}{\pi m_1}}\right] \quad (1)$$

where p_1 is the partial pressure of the target species, which for a nearly pure feed almost equals the total pressure; and m_1 is its molecular mass. The critical area in this case is simply the cross sectional area of the tube. This leads to a sublimation rate that is constant with time and proportional to the square of the tube radius.

The second mechanism involving mass transport in the collection tube is that of diffusion (6b in Table 1). When saturated vapor above the boat diffuses down a collection tube of length L, the flux is

$$j_1 = \frac{D}{L}c_1 = \frac{D}{L}\left(\frac{p_1 m_1}{k_B T}\right) \quad (2)$$

where D is the Knudsen diffusion coefficient given by[10]

$$D = \frac{du_1}{3} = \frac{d}{3}\left[\sqrt{\frac{8k_B T}{\pi m_1}}\right] \quad (3)$$

and d is the diameter of the collection tube. This relation holds only if the mean free path in the vapor is much larger than the diameter of the collection tube; that is, if the Knudsen number is large. Again, the important area is the cross sectional area of the tube. This also yields a sublimation rate which is constant with time; however, the rate is proportional to the tube radius cubed.

The final mechanism where transport in the tube is controlling is that of viscous flow (6c in Table 1). The laminar velocity is

$$v_1 = \frac{p_1 d^2}{32\mu L} \quad (4)$$

where μ is the viscosity given by

$$\mu = \frac{2}{3\pi^{3/2}}\frac{\sqrt{m_1 k_B T}}{\sigma^2} \quad (5)$$

The overall flux j_1 is

$$j_1 = \left[\frac{p_1 m_1}{2k_B T}\right] v_1 \quad (6)$$

where the quantity in square brackets is the average concentration. Once again, the critical area is that of the tube cross section and the sublimation rate is constant with time. In this

Table 1. Key Equations for Different Sublimation Mechanisms

	Rate-Limiting Step	State of Solid	Key Area	Flux j_1
1	Diffusion in solid	Impure particles	Particles	$\sqrt{\frac{D^{\text{solid}}}{\pi t}}c_1^{\text{solid}}$
2	Diffusion through ash	Mixed particles	Particles or boat	$\sqrt{\frac{D^{\text{ash}} c_1^{\text{solid}} c_1^{\text{vapor}}}{2t}}$
3	Surface desorption	Nearly pure particles	Particles	kc_1^{solid}
4	Diffusion away from particles	Nearly pure particles	Particles	$\frac{2D^{\text{vapor}} c_1^{\text{vapor}}}{r}$
5	Mass transfer away from boat	Nearly pure particles	Boat	kc_1^{vapor}
6a	Hertz–Knudsen	Nearly pure particles	Tube	$\frac{c_1 u_1}{4}$
6b	Vapor diffusion	Nearly pure particles	Tube	$\frac{D^{\text{vapor}} c_1^{\text{vapor}}}{L}$
6c	Viscous flow	Nearly pure particles	Tube	$c_1 v_1$

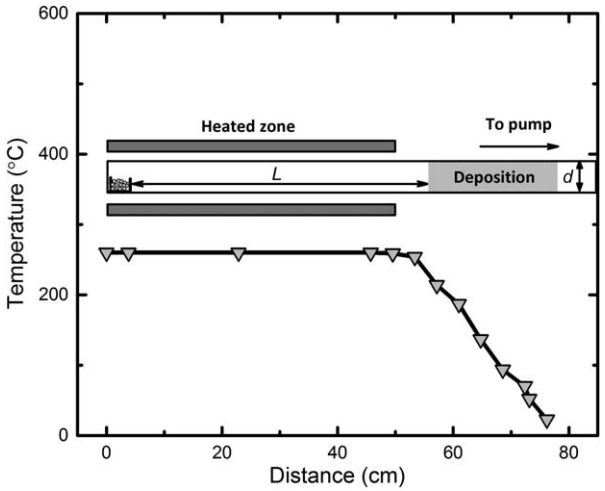

Figure 2. Temperature profile of the sublimation system.

The temperature drop is linear outside of the heated region.

case, the sublimation rate is proportional to the tube radius to the fourth power.

From the characteristic equations for each of the mechanisms in Table 1, the variation of the sublimation rate can be calculated as if each was separately rate controlling. For feeds of varying purity, the first four mechanisms are expected to yield a sublimation rate that is nonlinear in time, whereas the last four mechanisms predict a rate which is linear in time. Only the last three mechanisms predict that the rate will vary with collection tube radius and only the last two show a dependence on the tube length. These predictions are compared with the sublimation experiments described in the next section.

Experimental

Materials synthesis

α-NPD was chosen as a model material due to its wide commercial availability and use as a traditional standard in organic electronics.[6–9] In addition to material obtained commercially from Sigma–Aldrich [99.3% pure by high pressure liquid chromatography (HPLC)], α-NPD was prepared by a palladium-catalyzed amination reaction over the course of three batches that followed the general synthetic protocol described in Supporting Information. These batches were combined to give 206 g of α-NPD that was analyzed by HPLC to be 99.2% pure. This material was used to conduct the sublimation rate experiments discussed in this article. To test the effect of purity on the hypothesized rate-controlling steps, a second batch of α-NPD was deliberately synthesized with significantly lower purity via an alternative synthetic route also described in Supporting Information, yielding 37 g of product that was identified as 77.5% α-NPD by HPLC.

Sublimation

As described above, the rate of sublimation of α-NPD was measured under a variety of process conditions. The apparatus used, shown schematically in Figure 1, consists of a quartz collection tube in a furnace. One end of the tube contains α-NPD in an open boat. The boats used have a constant width of 3 cm with a length varying from 3.8 to 25 cm. All glassware used during experimentation was thoroughly cleaned using a 3:1 sulfuric acid and 30% hydrogen peroxide etch followed by a 500°C bake under vacuum. After loading each sample, the system was allowed to pump down to a base pressure of 10^{-5} Pa at 120°C in order to remove any remaining solvents. The temperature of the tube was 260°C where the tube was radiantly heated, but dropped linearly at the end of the heated zone, as shown in Figure 2. This linear drop is consistent with heat transfer occurring only by conduction along the walls of the tube. It is inconsistent with the more nearly exponential drop expected from a cooling fin.

Analytical

Sample purity both before and after sublimation was characterized using HPLC and mass spectroscopy. Purity of the materials was determined by HPLC area percent assay. Structural confirmation of α-NPD and major synthesis impurities was performed with a combination of mass electrospray ionization mass spectrometry and electrospray ionization tandem mass spectrometry (ESI-MS/MS). In depth analytical procedures and MS data are presented in Supporting Information.

Results

The primary impurities observed in the 99.2% α-NPD, shown in Figure 3, were readily removed using a single sublimation purification, yielding a product >99.9% pure by HPLC. Even in the case of impure (77.5%) starting material, a product with over 99% α-NPD by HPLC was produced. These results are summarized in Table 2. The product purity was found not to depend on the process conditions as studied in this article, but only on the initial purity. The ease of this separation is attributed to the significant difference in molecular weight between α-NPD and its primary impurities. Interestingly, when a feed that is 77.5% pure α-NPD is used, the rate is within experimental error of that observed with the purer feed, although the resulting product was less pure.

The amount sublimed is directly proportional to time, as shown by the sublimation data presented in Figure 4. In other words, the sublimation rate is not a function of time. This is inconsistent with the first four mechanisms presented in Table 1. This indicates that sublimation of α-NPD is not controlled by diffusion within particles or ash, by surface desorption, or by diffusion away from particles.

The amount sublimed was also found to be independent of particle size and material loading depth in the boat. To study the effect of particle size, powder with an average particle size on the order of 10 μm used in most experiments was compressed in a 10 ton press to make pellets 1 cm in diameter and 2–3 mm in height. Starting with the same initial mass, the α-NPD pellets were found to sublime at the same rate as the loose powder. These tightly pressed pellets provided an extreme test for any dependence on particle size. In the same sense, the depth or initial loading of particles in the boat has no effect, as shown by the data in Figure 5a. In this figure, the mass sublimed is plotted as a function of the initial mass loaded into the 3.8-cm long boat. Although the initial mass varies by a factor of four, the sublimation rate varies by about ± 10%, which is within the experimental error. Again these results show that the sublimation of α-NPD is not limited by the first four mechanisms in Table 1.

At the same time, the length and especially the diameter of the collection tube are found to affect the sublimation

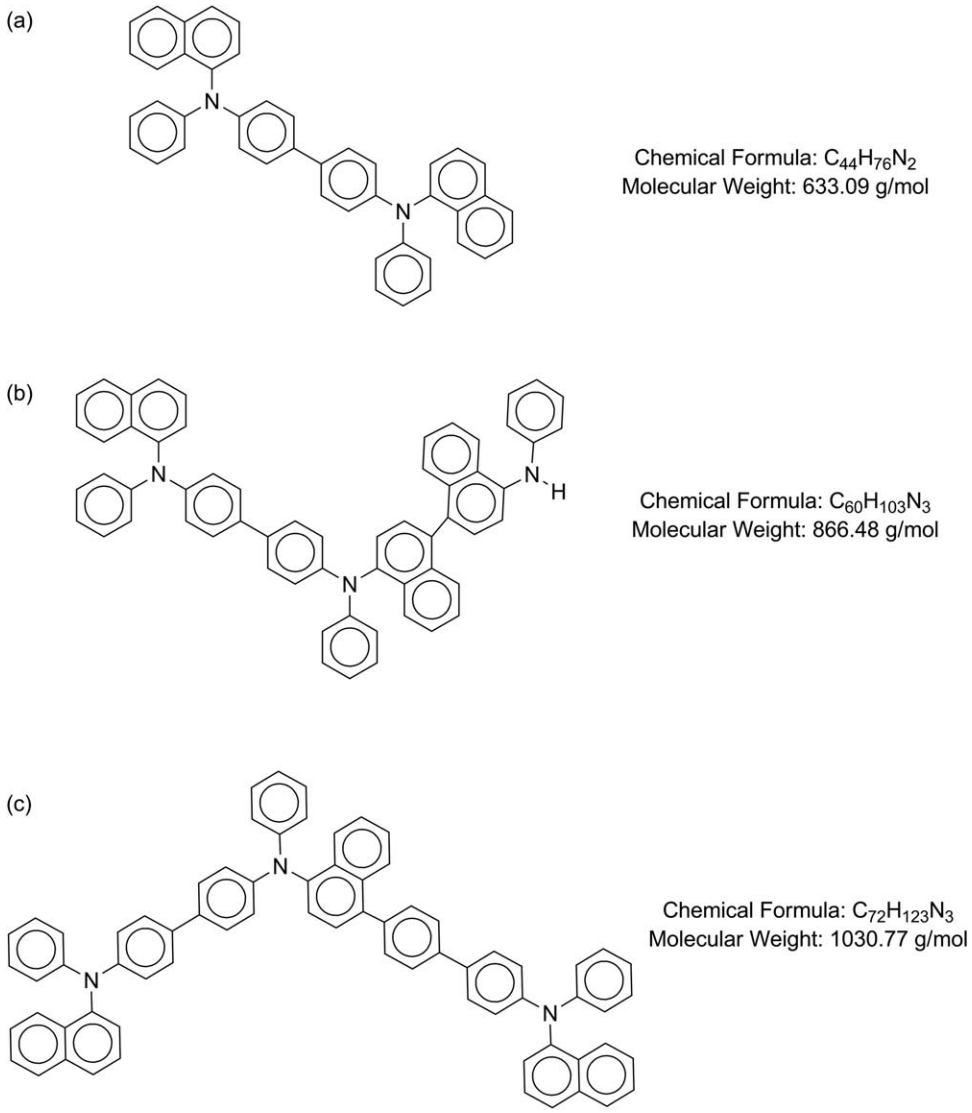

Figure 3. (a) Molecular structure for α-NPD and (b, c) Primary impurities.

rate. The effect of tube length can already be inferred from the data in Figure 4. In particular, the mass sublimed for the 25-cm boat is systematically greater than that for the 3.8-cm boat. This arises from minor differences in experimental geometry. As the boats are always placed at the extreme of the hot end of the collection tube, the center of the largest boat is implicitly placed closer to the cold end than the center of the smallest boat. Thus, vapor sublimed from the larger boat travels a shorter distance to reach the collection zone. This causes the systematic difference shown in Figure 4.

To examine this more directly, sublimation rates were measured for the 3.8-cm boat placed at different distances from the collection zone. The results, shown in Figure 5b, show that larger sublimation rates occur at smaller distances. This dependence on transport length is not predicted by the Hertz–Knudsen equation, but instead is consistent with both flow and diffusion.[10] However, reducing the distance sublimed by a factor of two increases the sublimation rate by only a factor of 1.4, less than the factor of two predicted for diffusion or flow, that is, by Eqs. 2 and 6. The results for sublimation with different collection tube diameters, shown in Table 3 and Figure 6, are much more definitive. They indicate that the sublimation rate varies with the square of the collection tube diameter. This seems consistent with the Hertz–Knudsen equation, and not with Knudsen diffusion or with viscous flow. However, this conclusion is less exact than it first appears, as discussed in the first section of the discussion.

Table 2. Purity of α-NPD Before and After Sublimation

Material Source	Initial Purity (%)	After Purification (%)
Sigma–Aldrich	99.3	99.9
Dow	99.2	99.9
Dow	71	99.0

High purity was achieved even for impure starting material.

The sublimation rate is a strong function of the temperature, as shown by the data in Table 3. This is the result of the vapor pressure of α-NPD, which when measured by an isothermal thermogravimetric effusion method[18] at temperatures from 325 to 425°C varies as

$$p_1, Pa = 1.1 \cdot 10^{12} e^{\frac{-14952}{(T,K)}} \quad (7)$$

If Eq. 16 is extrapolated to the lower temperatures used here, the vapor pressure is 0.7 Pa at 260°C, and about 10

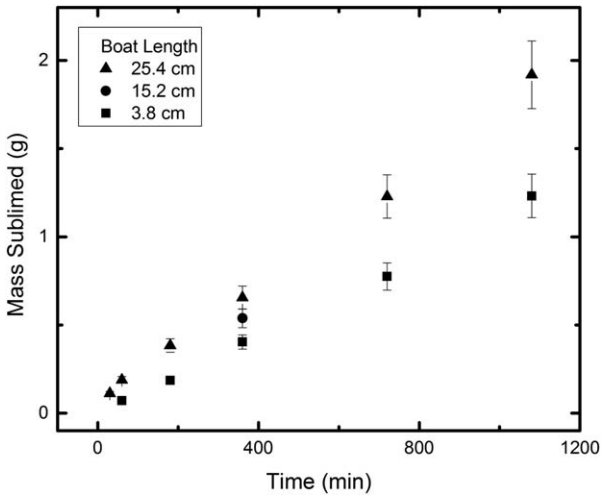

Figure 4. Mass sublimed with respect to time for various source boat lengths.

Mass sublimed is linear with respect to time. The difference in slope is due to a change in transport length dictated by the system geometry, not an increase in boat area.

times larger at 290°C. This is roughly the increase observed, even though the extrapolation is over 50 times below the smallest vapor pressure measured.

Discussion

Although the results clearly show that mass transfer down the tube is the rate-limiting step for sublimation, the exact mechanism is less clear. This section explores the possible mechanisms in more detail, speculating on the detailed physics involved and then discussing methods by which this process could be scaled up.

Table 3. Sublimation Rate Data for Various Operating Temperatures and Tube Diameters

Temperature (°C)	Tube Diameter (cm)	Sublimation Rate (g/h)
260	2.3	0.036
260	3.0	0.067
260	3.5	0.090
290	2.3	0.594
290	3.0	0.967

Sublimation rate increases exponentially with temperature and linearly with the square of tube diameter.

Sublimation mechanism

To determine the exact mechanism for mass transport down the tube, it is important to note that the total mass sublimed per unit time is constant between the sample boat and the start of the collection zone. The mass flux, which is a product of the density ρ and the velocity v_1, is also constant. Thus by a mass balance, the sublimation rate should vary with the cross sectional area of the collection tube, and hence with the tube radius squared. This is consistent with the results in Table 3 and Figure 6. However, while ρv_1 is constant, the detailed variations of ρ and v_1 are unknown. For example, for α-NPD at 260°C in the 3-cm diameter collection tube, the sublimation rate is 0.067 g/h, so ρv_1 is 2.6×10^{-5} kg/m^2 s. Calculating the Reynolds number for this case yields $\mathrm{Re}=\frac{\rho v_1 d}{\mu}=0.23$, indicating that the flow is laminar. At the same time, the Knudsen number, which is simply the ratio of mean free path λ and the tube diameter d, can be calculated by approximating the collision diameter σ of α-NPD as 2 nm based on its molecular structure. At the tube inlet, this is $Kn=\frac{\lambda}{d}=\frac{k_B T}{\sqrt{2}\pi\sigma^2 p d}=0.1$. This result implies that at

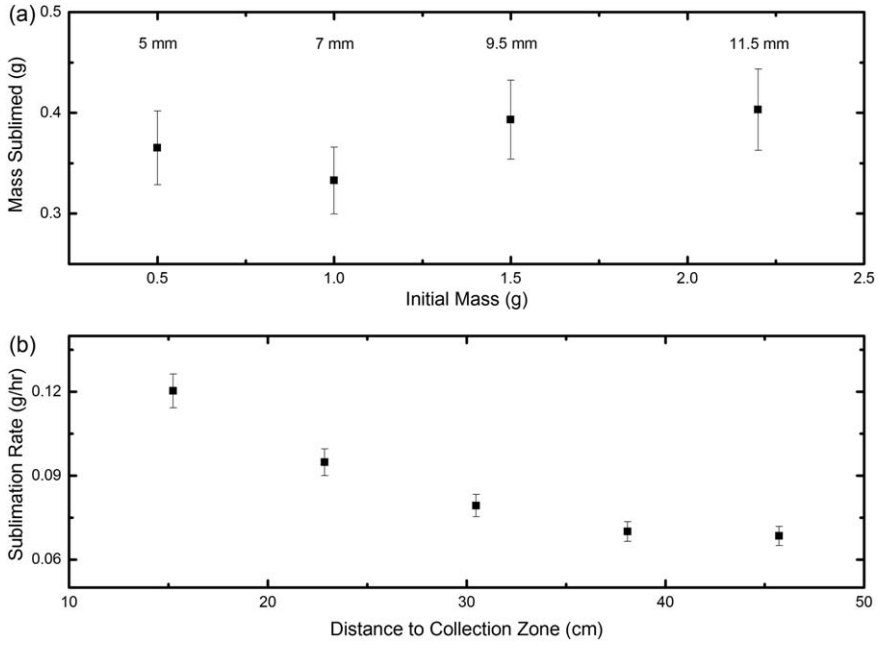

Figure 5. (a) Mass sublimed after 6 h for various initial charges of α-NPD.

The numbers above the data represent the initial depth of material in the sample boat. Sublimation rate is independent of initial loading.

(b) Sublimation rate as a function of the distance to the collection zone.

The rate increases as the distance to the collection zone decreases, signifying a dependence on transport down the tube.

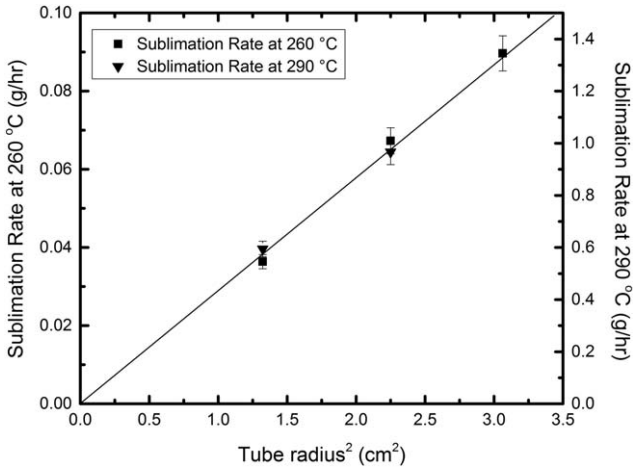

Figure 6. Sublimation rate as a function of the tube radius.

The data are presented on two axes to account for the temperature dependence of vapor pressure. The rate is proportional to the square of the tube radius.

the inlet many collisions are intermolecular, but that collisions at the wall are frequent enough to cause some slip.[19–21] Farther down the tube, Knudsen diffusion will be still more important and slip will be larger. Finally, once the vapor enters the collection zone, material begins to stick to the wall and deposition becomes important.

These considerations suggest that there are multiple mechanisms behind mass transport in the tube. More specifically, they suggest that between the boat and deposition zone, laminar flow and Knudsen diffusion occur in parallel. Both these transport mechanisms are inversely proportional to the distance between the boat and the deposition zone. In addition, after these parallel mechanisms, there is in series a resistance due to deposition R_{Dep}. Thus

$$\frac{\text{Total Vapor Pressure}}{\text{Total Mass Flux}} = R_{\mathrm{Dep}} + \frac{L}{\frac{L}{R_{\mathrm{Flow}}} + \frac{L}{R_{\mathrm{Dif}}}} \tag{8}$$

This expectation is tested in Figure 7. The positive intercept on this plot is the sublimation expected at zero tube length, which is the contribution of deposition. The changes at finite length are the reduction in sublimation rate caused by finite flow and diffusion rates down the tube: the slower the flow and diffusion, the slower the sublimation.

With additional approximations, the data in Figure 7 can be compared with values expected from the theory outlined above. To begin, we assume that whatever flows exist follow the Hagen–Pouseille relation[22–24] (Eqs. 4–6) and Fick's Law (Eqs. 2 and 3). Then, note that the flux in the collection tube is

$$j_1 = \left\{ \frac{d}{3}\sqrt{\frac{8m_1}{k_{\mathrm{B}}T} + \frac{p_1 m_1 d^2}{64\mu k_{\mathrm{B}}T}} \right\} \frac{(p_1 - p_{1\mathrm{c}})}{L} = \left\{ \sqrt{\frac{m_1}{2k_{\mathrm{B}}T}} \right\} p_{1\mathrm{c}} \tag{9}$$

where p_{1c} is the pressure at the start of the collection zone. Thus, $(p_1 - p_{1c})$ is the pressure difference responsible for flow, whereas $(p_{1c}/k_{\mathrm{B}}T)$ is the concentration for deposition. The deposition process can be modeled using the equations developed by Hertz and Knudsen, which is often called physical vapor deposition[15–17,25,26] and is based on the total number of molecules impacting the surface for a given vapor concentration. Eliminating the unknown pressure p_{1c} and rearranging yields

$$\frac{1}{\left(\frac{\pi}{4}d^2\right)j_1} = \left[\frac{1}{\frac{\pi}{4}d^2 p_1}\sqrt{\frac{2RT}{\tilde{M}_1}}\right] + \left\{\frac{1}{\frac{\pi}{4}d^2 p_1}\left(\frac{1}{\frac{d}{3}\sqrt{\frac{8\tilde{M}_1}{\pi RT} + \frac{d^2\tilde{M}_1 p_1}{64\mu RT}}}\right)\right\} L \tag{10}$$

where the Boltzmann constant and the mass per molecule have been replaced with the gas constant and the molecular weight.

This result can be compared directly to experiment because the quantity in square brackets of Eq. 10 is the intercept in Figure 7, and the quantity in braces is the slope shown in that figure. For the conditions given above, the experimental intercept of 5 h/g is compared with the theoretical value of 0.4 h/g. In other words, the experimental flux for physical vapor deposition is 10 times less than the theory. This discrepancy, similar to that seen in many inorganic systems, was first observed for Hg by Hertz.[15] It was rationalized by Knudsen[16] through the introduction of a sticking coefficient, that is, the fraction of incident molecules which are incorporated into the solid. From this, the sticking coefficient of α-NPD is approximately 0.1, which is similar to those observed in other systems.[17]

The slope of inverse total flux vs. tube length L is seen from Figure 7 to be about 37 h/g m. That found from Eq. 9 is 15 h/g m. Due to the approximations involved, we do not argue that this is exact, but only that it is consistent with the mechanism proposed. This provides a sharper image of the physics behind this sublimation than previously held.

Scale-up of purification by sublimation

Using this basic understanding of the mechanism, processes for increasing the productivity of small scale sublimation can be considered. This can be done by improving the existing batch process, or by switching to a more continuous operation. Both strategies will be considered.

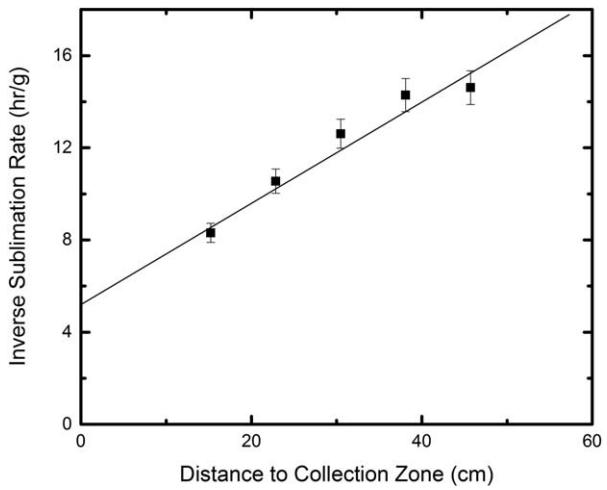

Figure 7. Plotting the inverse sublimation rate against the distance to the collection zone separates the resistance due to transport from the resistance due to deposition.

The slope represents the transport component and the y-intercept represents the deposition component.

To scale-up the existing process, consider increasing the temperature and the diameter of the collection tube. Increasing the temperature does not significantly increase the molecular velocity, but it exponentially increases the vapor pressure and so the sublimation flux. For example, an increase in temperature from 260 to 290°C increases the vapor pressure of α-NPD by a factor of 10, making the sublimation 10 times more productive. Although it provides a sharply increased vapor pressure, higher temperature risks degradation of the active material. Although degradation was found to be minimal in these experiments, it could be more serious for other compounds and must be evaluated on a case by case basis. Increasing the diameter of the collection tube gives an increase that is proportional to the square of the tube radius. However, the tube diameter should not greatly exceed the tube length, because then larger amounts of impurities may be more difficult to remove. Reducing the tube length will not normally give large increases in sublimation rate.

To test these generalizations, data were obtained from an industrial sublimation unit operated by The Dow Chemical Company. A similar system geometry was used with a comparable organic material at a temperature such that its vapor pressure was 100 times that of those in this study. The tube diameter was increased from 0.030 to 0.30 m, so that the area increased by a factor of 100. The length was reduced from 0.46 to 0.10 m, increasing the rate two times. This suggests an increase in sublimation rate 20,000 times larger than that of the system used for this study, from 0.067 g/h to over 1000 g/h. This estimate agrees with the data obtained from Dow.

These experiments also suggest ways in which sublimation can be operated more continuously. The obvious way is to pump an inert carrier gas like nitrogen or argon at higher pressures through a packed bed of small particles of the active material to produce a vapor which is at least 30% saturated. This vapor is then cooled to form purified crystals. Such a process can easily use a convective velocity of 10 m/s or greater, and so has the potential to have a rate of over a factor of 10 greater than the batch processes described in this article. Such a process is sometimes called "entrainer sublimation[27]" and is often used to grow large single crystals of organic molecules.[28] Reaching this potential will hinge on carefully designing the zone of the sublimator where the crystals are collected. Because the vapor is moving rapidly and may have slower mass transfer than in the low pressure gas used currently, this zone should be longer and probably offer more surface area.[29,30] At the same time, it should still allow the crystals to be harvested easily. This may be difficult to achieve and may be less attractive than more conventional, large batch operations.

Acknowledgments

Funding and support for this work was provided by the Dow Chemical Company. The authors thank Jacob Crosthwaite and Lynn Stiehl for the vapor pressure data and acknowledge useful discussions with Dr. John Pendergast and Dr. Matthew Grandbois. R.J.H. is a member of the Dow Chemical Company Technical Advisory Board.

Notation

A = area
c_1 = concentration
d = collection tube diameter
D = diffusion coefficient
j_1 = flux
k = rate constant for mass transfer
k_B = Boltzmann constant
Kn = Knudsen number
l = ash thickness
L = collection tube length
m_1 = molecular mass
M = mass
$\tilde{M}_1$ = molecular weight
p_1 = partial pressure
r = radius of particle
R = gas constant
Re = Reynolds number
R_{Dep} = resistance due to deposition
R_{Dif} = resistance due to diffusion
R_{Flow} = resistance due to flow
t = time
T = temperature
u_1 = molecular velocity
v_1 = convective velocity
λ = mean free path
μ = viscosity
ρ = density
σ = collision diameter

Literature Cited

1. Tang CW, VanSlyke SA. Organic electroluminescent diodes. *Appl Phys Lett*. 1987;51:913–915.
2. Hung LS, Chen CH. Recent progress of molecular organic electroluminescent materials and devices. *Mater Sci Eng R*. 2002;39: 143–222.
3. Xiao L, Chen Z, Qu B, Luo J, Kong S, Gong Q, Kido J. Recent progresses on materials for electrophosphorescent organic light-emitting devices. *Adv Mater*. 2011;23:926–952.
4. McGhie AR, Garito AF, Heeger AJ. A gradient sublimer for purification and crystal growth of organic donor and acceptor molecules. *J Cryst Growth*. 1974;22:295–297.
5. Roberson LB, Kowalik J, Tolbert LM, Kloc C, Zeis R, Chi X, Fleming R, Wilkins C. Pentacene disproportionation during sublimation for field-effect transistors. *J Am Chem Soc*. 2005;127: 3069–3075.
6. VanSlyke SA, Chen CH, Tang CW. Organic electroluminescent devices with improved stability. *Appl Phys Lett*. 1996;69:2160–2162.
7. O'Brien DF, Burrows PE, Forrest SR, Koene BE, Loy DE, Thompson ME. Hole transporting materials with high glass transition temperatures for use in organic light emitting devices. *Adv Mater*. 1998;10:1108–1112.
8. Forsythe EW, Abkowitz MA, Gao Y. Tuning the carrier injection efficiency for organic light-emitting diodes. *J Phys Chem B*. 2000; 104:3948–3952.
9. Tse SC, Kwok KC, So SK. Electron transport in naphthylamine-based organic compounds. *Appl Phys Lett*. 2006;89:262102–262102-3.
10. Cussler EL. *Diffusion: Mass Transfer in Fluid Systems*, *3rd ed*. Cambridge: Cambridge University Press, 2009.
11. Schultz RD, Dekker AO. The effect of physical adsorption on the absolute decomposition rates of crystalline ammonium chloride and cupric sulfate trihydrate. *J Phys Chem*. 1956;60:1095–1100.
12. Chaiken RF, Sibbett DJ, Sutherland JE, Van de Mark DK, Wheeler A. Rate of sublimation of ammonium halides. *J Chem Phys*. 1962; 37:2311–2318.
13. Langmuir I. The evaporation of small spheres. *Phys Rev*. 1918;12: 368–370.
14. Readey DW, Kuczynski GC. Sublimation of aluminum oxide in hydrogen. *J Am Ceram Soc*. 1966;49:26–29.
15. Hertz H. On the evaporation of liquids, especially mercury, in vacuo. *Ann Phys (Leipzig)*. 1882;17:177–198.
16. Knudsen M. Maximum rate of vaporization of mercury. *Ann Phys (Leipzig)*. 1915;47:697–705.
17. Sherwood TK, Cooke NE. Mass transfer at low pressures. *J Am Inst Chem Eng*. 1957;3:37–42.
18. OECD. *Test No. 104: Vapour Pressure*, OECD Guidelines for the Testing of Chemicals, Section 1, OECD Publishing, 2006.
19. Arkilic EB, Schmidt MA, Breuer KS. Gaseous slip flow in long microchannels. *J Microelectromech Syst*. 1997;6:167–178.

20. Shen S, Chen G, Crone RM, Anaya-Dufresne M. A kinetic-theory based first order slip boundary condition for gas flow. *Phys Fluids*. 2007;19:086101–086101-6.
21. Lorrode FE, Housiadas C, Drossinos Y. Slip-flow heat transfer in circular tubes. *Int J Heat Mass Transfer*. 2000;43:2669–2680.
22. Harley JC, Huang Y, Bau HH, Zemel JN. Gas flow in microchannels. *J Fluid Mech*. 1995;284:257–274.
23. Van den Berg HR, Ten Seldam CA, van der Gulik PS. Compressible laminar flow in a capillary. *J Fluid Mech*. 1993;246:1–20.
24. Prud'Homme RK, Chapman TW, Bowen JR. Laminar compressible flow in a tube. *Appl Sci Res*. 1986;43:67–74.
25. Rahimi P, Ward CA. Kinetics of evaporation: statistical rate theory approach. *Int J Thermodyn*. 2005;8:1–14.
26. Shtein M, Gossenberger HF, Benziger JB, Forrest SR. Material transport regimes and mechanisms for growth of molecular organic thin films using low pressure organic vapor phase deposition. *J Appl Phys*. 2001;89:1470–1476.
27. Mullin JW. *Crystallization*, *4th ed*. Oxford: Butterworth-Heinemann, 2001.
28. Kloc C, Simpkins PG, Siegrist T, Laudise RA. Physical vapor growth of centimeter-sized crystals of α-hexathiophene. *J Cryst Growth*. 1997;182:416–427.
29. Jeon H-G, Inoue M, Hiramatsu N, Ichikawa M, Taniguchi Y. A modified sublimation purification system using arrays of partitions. *Org Electron*. 2008;9:903–905.
30. Jeon H-G, Kondo Y, Maki S, Matsumoto E, Taniguchi Y, Ichikawa M. A highly efficient sublimation purification system using baffles with orifices. *Org Electron*. 2010;11:794–800.

Manuscript received Aug. 19, 2013, and revision received Jan. 5, 2014.